

Article

Highly Loaded Mesoporous Ni–La₂O₃ Catalyst Prepared by Colloidal Solution Combustion Method for CO₂ Methanation

Guoli Tang ^{1,†}, Dandan Gong ^{1,†}, Hui Liu ² and Luhui Wang ^{1,*} 

¹ Department of Chemical Engineering, School of Petrochemical Technology and Energy Engineering, Zhejiang Ocean University, Zhoushan 316022, Zhejiang, China; tang15070212@zjou.edu.cn (G.T.); dandangong@zjou.edu.cn (D.G.)

² School of Food and Pharmaceutical, Zhejiang Ocean University, Zhoushan 316022, Zhejiang, China; liuhui@zjou.edu.cn

* Correspondence: wangluhui1008@zjou.edu.cn; Tel.: +86-580-255-1050

† These authors contributed equally to this work.

Received: 1 April 2019; Accepted: 7 May 2019; Published: 11 May 2019



Abstract: Highly dispersed Ni-based catalysts for CO₂ methanation have been extensively studied over the last decade. However, a highly loaded Ni-based catalyst always results in a large Ni particle size and poor CO₂ methanation activity. In this work, a colloidal solution combustion method was used to prepare a highly loaded Ni–La₂O₃ catalyst (50 wt % Ni) with a small Ni particle size and abundant metal–support interface. The characterizations demonstrated that a Ni–La₂O₃ catalyst prepared in this way has a mesoporous structure and a small Ni particle size. Due to the small Ni particle size and abundant metal–support interface, the highly loaded mesoporous Ni–La₂O₃ catalyst exhibits higher activity and selectivity in CO₂ methanation compared to the Ni–La₂O₃ catalyst prepared by a conventional solution combustion method.

Keywords: highly loaded Ni catalyst; La₂O₃; colloidal solution combustion; CO₂ methanation

1. Introduction

CO₂ emissions have increased rapidly due to the increasing consumption of fossil fuels, resulting in global warming and climate change. Various methods were proposed to convert CO₂ to fuels and chemicals [1,2]. CO₂ methanation is a promising reaction for converting greenhouse gas CO₂ and renewable H₂ into methane [3]. Moreover, the produced methane is an important chemical intermediate that can be used in chemical and petrochemical industries. CO₂ methanation, commonly called the Sabatier reaction, is an exothermic reaction which is thermodynamically favored at low temperatures [3,4]. However, since CO₂ molecules have high chemical inertia, the CO₂ methanation reaction activity is very low at a low temperature and atmospheric pressure.



To realize low temperature CO₂ methanation, various catalysts have been designed, developed, and tested for their catalytic activity at a low temperature. Many metal catalysts, such as supported Rh [5,6], Ru [7], Pd [8], Co [9–11], and Ni [12–14] catalysts, have been developed for CO₂ methanation. Among the reported catalysts, supported Ni-based catalysts have been intensively studied due to their low price and high levels of activity.

To increase the low-temperature activity of Ni-based catalysts, many methods have been proposed for preparing catalysts with a small Ni particle size [15]. A general strategy for increasing the dispersion

of active components involves loading the active component on a carrier with a high surface area, such as mesoporous silica [16–18]. However, the metal loading of a catalyst prepared using this method is low, and usually not higher than 30 wt %.

Metal loading and particle size are the two most important parameters in determining the catalytic performance for CO₂ methanation. It would be ideal if the two parameters could be independently controlled. However, in reality, a catalyst with a higher loading usually has a larger particle size [19] and exhibits low activity. This interdependence between metal loading and particle size hinders the preparation of a highly active CO₂ methanation catalyst with high Ni loading.

La₂O₃ has been widely used as a promoter or support in CO₂ conversion catalysts, such as CO₂ methanation and dry reforming of methane (DRM), due to its strong adsorption of CO₂ [20]. Song et al. [21] reported that 10% Ni/La₂O₃ catalysts prepared by the impregnation method were active in CO₂ methanation. Li et al. [22] reported that La₂O₂CO₃ nanorods could be used as support precursors to Ni/La₂O₃ nanorod catalysts with stabilized Ni nanoparticles. LaNiO₃ perovskite can be used as precursors to produce highly dispersed Ni-based catalysts. However, this requires high-temperature reduction. To the best of our knowledge, although some mesoporous supports, such as Al₂O₃, SiO₂, and ZrO₂, have been used in CO₂ methanation catalysts, mesoporous Ni–La₂O₃ catalysts have not been reported for CO₂ methanation.

Herein, a colloidal solution combustion method, which had been previously used to prepare mesoporous CeO₂ and CeO₂-based catalysts [23,24], was proposed to prepare highly loaded Ni on La₂O₃. By using this method, a highly loaded Ni–La₂O₃–M (~50 wt % Ni) catalyst with a small Ni particle size was synthesized. The catalyst has an abundant metal–support interface and exhibits good catalytic performance in CO₂ methanation.

2. Results and Discussion

2.1. Characterization of Catalysts

N₂ adsorption–desorption isotherms and pore size distribution curves of 50% Ni–La₂O₃–M and 50% Ni–La₂O₃ are shown in Figure 1. According to the International Union of Pure and Applied Chemistry (IUPAC) classification, the fresh, reduced, and used 50% Ni–La₂O₃–M catalysts exhibit the typical IV type isotherms which are associated with capillary condensation in mesoporous materials [25]. The result indicates that after being treated with a hot NaOH solution, SiO₂ was etched and a mesoporous structure was formed. However, the fresh 50% Ni–La₂O₃ catalyst showed the typical III type isotherms with no inflection point on the curve, indicating weak interactions with the adsorbate of N₂. Figure 1b shows that the 50% Ni–La₂O₃–M catalyst has a relatively narrow pore size distribution, which was concentrated at about 16–20 nm. This indicates that the catalyst has a uniform mesoporous structure.

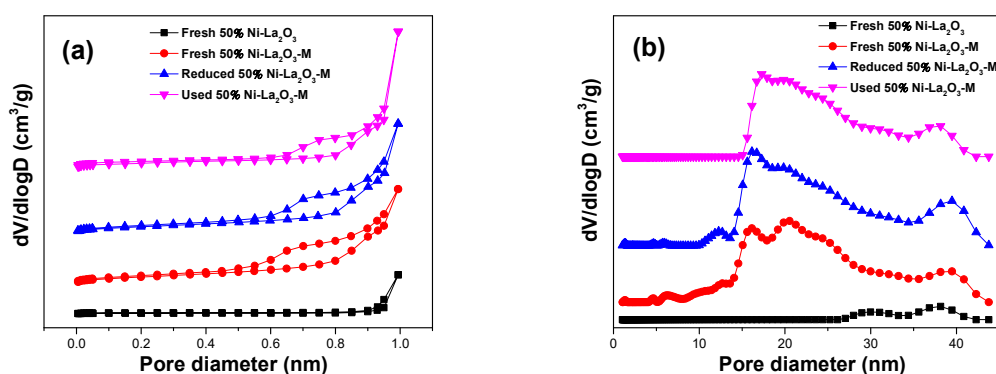


Figure 1. Nitrogen adsorption–desorption isotherms curves (a) and pore size distributions (b) of 50% Ni–La₂O₃–M and 50% Ni–La₂O₃.

The surface area, pore volume, and average pore size for these catalysts are listed in Table 1. It can be seen that the Brunauer–Emmett–Teller (BET) surface area of the fresh 50% Ni–La₂O₃–M is 70.4 m² g^{−1}, which is 8.8-fold higher than the fresh 50% Ni–La₂O₃ catalyst. The pore volume of the fresh 50% Ni–La₂O₃–M was higher than that of the fresh 50% Ni–La₂O₃ catalyst, which should have resulted from the etching of SiO₂ by NaOH during the preparation process. The average pore size of 50% Ni–La₂O₃ catalyst was 71 nm, which indicated that the catalyst has a mainly macroporous structure. It should be noted that the average pore size of 50% Ni–La₂O₃ catalyst was larger than those shown in Figure 1b. This is because quenched solid density functional theory (QSDFT) is only suitable for micropore and mesoporous analysis, but not for macropore analysis [26].

Table 1. Physical properties of 50% Ni–La₂O₃–M and 50% Ni–La₂O₃.

Samples	S _{BET} (m ² g ^{−1})	Pore Volume (cm ³ g ^{−1})	Average pore size (nm)
Fresh 50% Ni–La ₂ O ₃	7.2	0.13	71
Fresh 50% Ni–La ₂ O ₃ –M	70.4	0.32	18
Reduced 50% Ni–La ₂ O ₃ –M ^a	79.2	0.37	19
Used 50% Ni–La ₂ O ₃ –M ^b	55.5	0.45	16

^a The catalyst was reduced at 400 °C for 40 min in 20% H₂/Ar. ^b The catalyst was used at 300 °C for 50 h under methanation reaction conditions.

After the reduction and methanation reaction, the BET surface area and average pore size of 50% Ni–La₂O₃–M had a slight change. In summary, the 50% Ni–La₂O₃–M catalyst prepared by the colloid solution combustion method formed a mesoporous structure which has a high specific surface area and pore volume.

Figure 2 presents the X-ray diffraction (XRD) patterns of the fresh and reduced catalysts. For the fresh catalysts, the peaks at 37.2, 43.3, and 62.9° are attributed to NiO, which is consistent with the literature [27]. It is important to note that the peaks corresponding to LaNiO₃ with a perovskite structure, namely the peaks at 32.8, 47.3, and 58.6° [28], show up in 50% Ni–La₂O₃ catalysts, which indicates the excessively strong interaction between nickel and lanthanum. Furthermore, the peaks of NiO for 50% Ni–La₂O₃–M catalyst are weaker and wider than those in 50% Ni–La₂O₃, suggesting that 50% Ni–La₂O₃–M catalyst has a smaller particle size.

After reduction, the diffraction peaks corresponding to the crystalline NiO disappeared and the peaks of Ni appeared, indicating that NiO was successfully reduced. As shown in the gray shadow, the peaks of the LaNiO₃ perovskite were significantly weaker in the reduced 50% Ni–La₂O₃ compared to the fresh 50% Ni–La₂O₃. However, these peaks still existed, indicating that the LaNiO₃ perovskite in 50% Ni–La₂O₃ catalyst was only partially reduced at 400 °C. Meanwhile, the peaks of Ni in 50% Ni–La₂O₃–M were also weaker than those in 50% Ni–La₂O₃, revealing that the former has a smaller nickel particle size. The crystal sizes of NiO and Ni calculated by XRD results are listed in Table 2. In short, the XRD results indicate that using silica colloid as a template can form small NiO particle and amorphous La₂O₃ without formation of LaNiO₃.

Table 2. Crystallite particle size of Ni and NiO.

Catalysts	Crystal Size of NiO (nm)		Ni Crystal Size (nm) ^a
	By XRD ^a	By TEM ^b	
Fresh 50% Ni–La ₂ O ₃ –M	3.0	3.2	/
Reduced 50% Ni–La ₂ O ₃ –M	/	/	4.3
Used 50% Ni–La ₂ O ₃ –M	/	/	4.5
Fresh 50% Ni–La ₂ O ₃	7.0	6.8	/
Reduced 50% Ni–La ₂ O ₃	/	/	7.1

^a Calculated from XRD results based on Scherrer's equation. ^b Average NiO particle size was estimated from TEM.

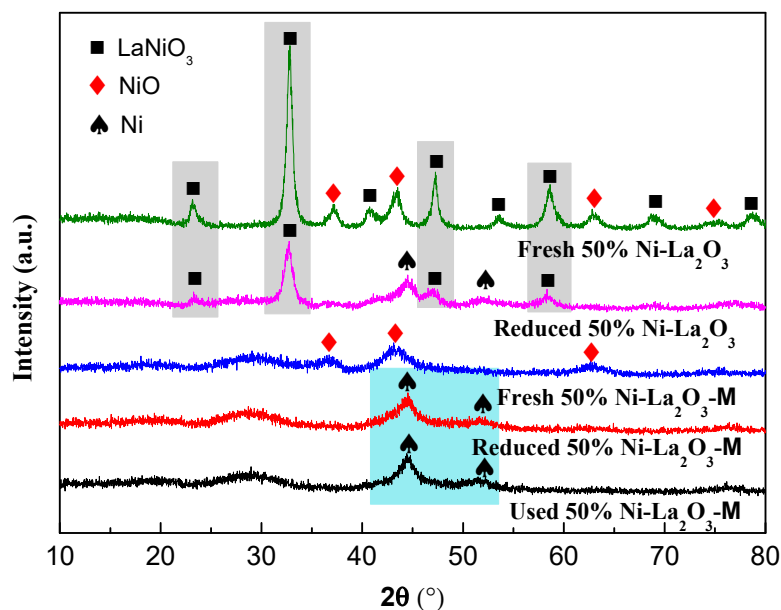


Figure 2. X-ray diffraction (XRD) patterns of 50% Ni-LaNiO₃-M and 50% Ni-LaNiO₃. Reduced catalysts were reduced at 400 °C for 40 min with 20% H₂/Ar. We used 50% Ni-LaNiO₃-M at 300 °C for 50 h in a CO₂ methanation reaction.

The transmission electron microscopy (TEM) and high-resolution transmission electron microscopy (HR-TEM) analysis provides information on the textural properties of the fresh catalysts created using different preparation methods. For 50% Ni-LaNiO₃-M catalysts, a well-ordered mesoporous structure with a pore size of around 18 nm was observed in Figure 3a,b, which is consistent with the N₂ adsorption–desorption results. The uniform pore size distribution of 50% Ni-LaNiO₃-M is due to the use of colloidal SiO₂ with a particle size of 20–22 nm during the preparation process. After the etching of SiO₂, mesopores were generated in the catalyst, and the pore size was associated with the particle size of colloidal SiO₂.

In Figure 3c shows a representative image for 50% Ni-LaNiO₃-M catalyst with a lattice distance of 2.08 Å belonging to NiO (200) that was observed [29]. After scanning a large number of pictures, we did not find any lattice distances corresponding to La₂O₃. The absence of crystalline La₂O₃ demonstrates that the majority of La₂O₃ exists in an amorphous form. This is consistent with the XRD results as there were no diffraction peaks of La₂O₃. As shown in Figure 3b,c, the pore wall was composed of NiO nanoparticles and amorphous La₂O₃, and most of the NiO nanoparticles were embedded by amorphous La₂O₃ in the pore walls.

On the contrary, the Ni-LaNiO₃ catalyst had a pore size of 50–100 nm, as shown in Figure 3d. As shown in Figure 3f, for the fresh 50% Ni-LaNiO₃, the lattice distances of 3.08 and 2.73 Å are attributed to La₂O₃ and LaNiO₃, respectively [30]. Meanwhile, the particles of NiO in 50% Ni-LaNiO₃ were larger than 50% Ni-LaNiO₃-M. The particle size distribution of NiO for these two catalysts are shown in Figure 3g,h. The average size of the NiO nanoparticles (NPs) for the fresh 50% Ni-LaNiO₃ and 50% Ni-LaNiO₃-M catalysts can be calculated from these two column charts. The sizes of NiO NPs for 50% Ni-LaNiO₃-M (around 3.2 nm) are smaller than those of 50% Ni-LaNiO₃ (around 6.8 nm), which is consistent with the XRD results.

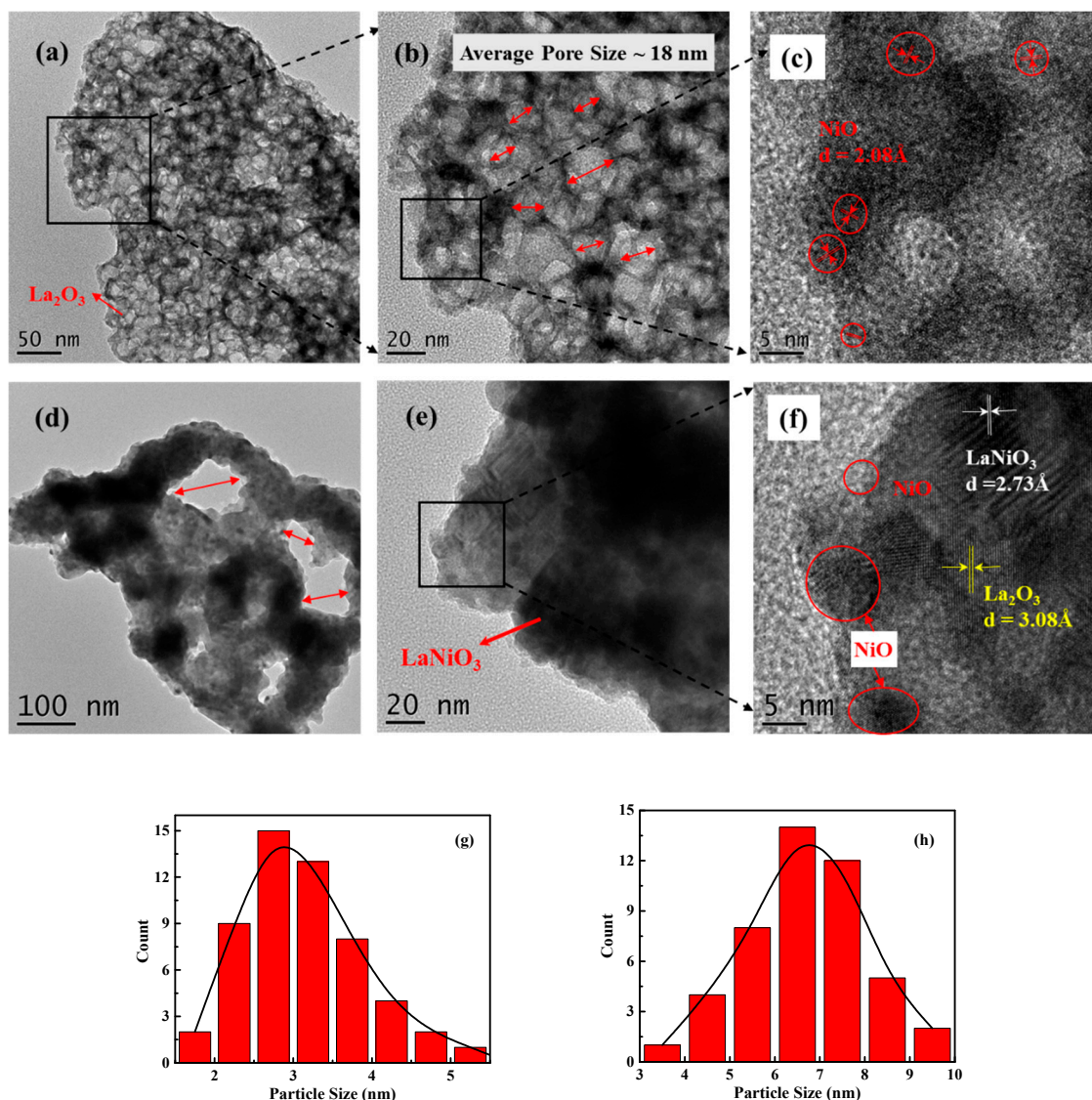


Figure 3. TEM images and NiO particle size distributions of fresh catalysts: (a–c,g) 50% Ni–La₂O₃–M and (d–f,h) 50% Ni–La₂O₃.

Figure 4 exhibits the H₂-temperature programmed reduction (H₂-TPR) profiles of these two fresh catalysts. For the fresh 50% Ni–La₂O₃–M, a reduction peak between 300 and 600 °C (centered on 400 °C) represents the reduction of NiO particles [31]. The 50% Ni–La₂O₃ catalyst has three distinct reduction peaks. The peaks at around 400 and 570 °C correspond to the reduction of Ni³⁺ to Ni²⁺ and Ni²⁺ to Ni⁰ in the perovskite lattice, respectively [32], which confirms the formation of LaNiO₃ perovskite. Furthermore, the peak at around 400 °C represents the reduction of Ni²⁺ to Ni⁰ in NiO nanoparticles. The oxygen vacancies in the lattice of LaNiO₃ might be responsible for the low-temperature peak appearing at 300 °C. The results indicate that the catalyst prepared without using colloid silica only resulted in partial formation of LaNiO₃ perovskite. In order to completely destroy the lattice and fully reduce metal nickel, the required reduction temperature is as high as 550 °C. It is significantly and comparatively easier to reduce the catalyst prepared by the colloidal solution combustion method due to the absence of LaNiO₃. This is consistent with XRD results.

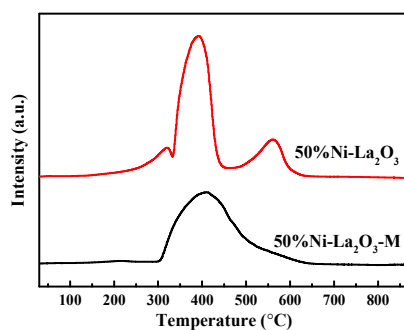


Figure 4. H₂-temperature programmed reduction (H₂-TPR) curves of 50% Ni-L₂O₃-M and 50% Ni-L₂O₃ catalysts.

The Ni dispersion measured by H₂-temperature programmed desorption (H₂-TPD) is listed in Table 3. The Ni dispersion of 50% Ni-L₂O₃-M is lower than that of 50% Ni-L₂O₃. The lower Ni dispersion of 50% Ni-L₂O₃-M should be attributed to the special embedded structure of the catalyst, in which most small Ni particles are embedded in the pore wall by amorphous La₂O₃. Although the Ni dispersion of the 50% Ni-L₂O₃-M is low, the 50% Ni-L₂O₃-M with a special Ni-embedded structure has a rich metal-support interface, which had been proven to be essential for the methanation reaction.

Table 3. Ni dispersion and turnover frequency (TOF) calculated from H₂-TPD results.

Catalysts	Ni Dispersion (%) ^a	TOF (× 10 ⁻³ s ⁻¹) ^b
50% Ni-L ₂ O ₃	6.93	4.0
50% Ni-L ₂ O ₃ -M	4.01	57.0

^a Calculated from H₂-temperature programmed desorption (H₂-TPD) results. ^b TOF (s⁻¹) represents the number of CO₂ molecules converted per Ni surface atom per second at 250 °C.

2.2. Catalytic Performance

The activity catalysts were tested in CO₂ methanation at temperatures of 250–450 °C. CO₂ conversion and CH₄ selectivity are shown in Figure 5a,b, respectively. Compared with 50% Ni-L₂O₃, the catalyst of 50% Ni-L₂O₃-M exhibited higher CO₂ conversion and CH₄ selectivity, indicating the latter is much more active than the former. For 50% Ni-L₂O₃-M catalysts, the highest CO₂ conversion of 76% was obtained at around 400 °C with a CH₄ selectivity of around 99.5%. CO₂ conversion of 50% Ni-L₂O₃-M decreased to 71% at 450 °C, which is limited by the thermodynamic equilibrium due to the CO₂ methanation reaction being an exothermic reaction. In the meantime, CH₄ selectivity decreased to 98%, which is caused by the accelerated generation of CO derived from the reverse water gas shift reaction. Similar variation trends in conversion and selectivity can also be observed for 50% Ni-L₂O₃ catalysts. Furthermore, it should be noted that the CO₂ conversion of 50% Ni-L₂O₃-M reached 51% at 300 °C, while 50% Ni-L₂O₃ only reached 9%, suggesting that the 50% Ni-L₂O₃-M catalyst has good low-temperature activity. As listed in Table 3, the turnover frequency (TOF) of 50% Ni-L₂O₃-M at 250 °C is 12-fold higher than that of 50% Ni-L₂O₃, which indicates that the small Ni particles embedded by La₂O₃ in 50% Ni-L₂O₃-M were more active than the Ni particles supported on La₂O₃ in 50% Ni-L₂O₃. Combined with the characterization results, it is shown that the special mesoporous embedded structure in 50% Ni-L₂O₃-M led to an abundant metal-support interface, thus increasing the catalytic activity.

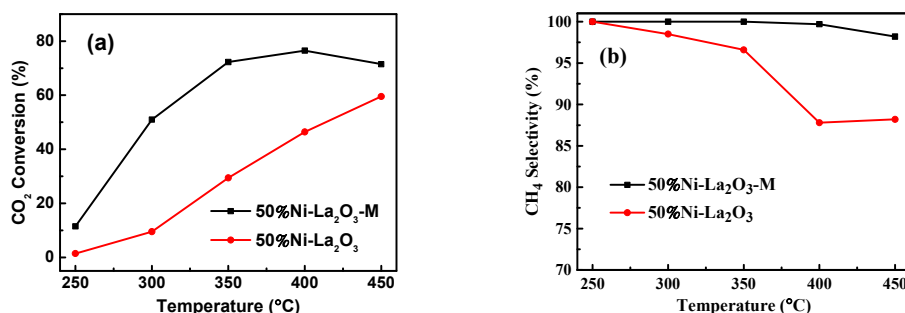


Figure 5. (a) CO₂ conversion and (b) CH₄ selectivity over 50% Ni-LaNiO₃-M and 50% Ni-LaNiO₃ in CO₂ methanation reaction at a gas hourly space velocity (GHSV) of 120,000 mL g⁻¹ h⁻¹ and 0.1 MPa in the gas mixture of H₂/CO₂/Ar = 4/1/5.

As shown in Figure 6, the stability test of 50% Ni-LaNiO₃-M was carried out at a high gas hourly space velocity (GHSV) of 120,000 mL g⁻¹ h⁻¹, and the temperature was set to 300 °C. CO₂ conversions of 50% Ni-LaNiO₃-M catalyst maintained stable catalytic performance throughout 50 h of testing. CO₂ conversion and CH₄ selectivity remained around 51% and 98%, respectively. This indicates that the La₂O₃-supported Ni catalyst prepared by the colloidal solution combustion method has excellent stability.

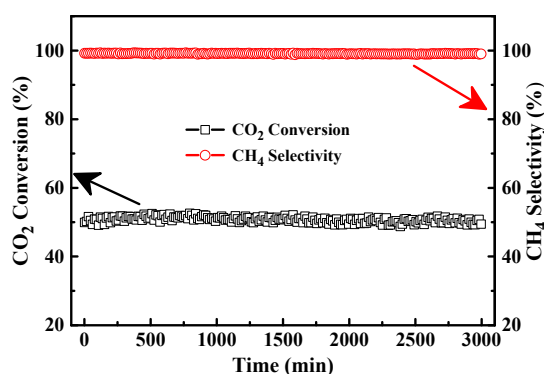


Figure 6. Stability of 50% Ni-LaNiO₃-M in CO₂ methanation reaction at GHSV = 120,000 mL g⁻¹ h⁻¹ on stream at 300 °C and 0.1 MPa in H₂/CO₂/Ar = 4/1/5.

The sintering and carbon deposition of Ni nanoparticles are the main reasons for the decline in catalyst performance during the stability test of CO₂ methanation. The chosen 50% Ni-LaNiO₃-M was characterized by XRD and TEM techniques. The absence of carbon nanotubes or nanofibers in TEM photographs (Figure 7) showed that no detectable carbon deposition occurred, meaning that no carbon was deposited on the surface of the catalysts. That is to say, 50% Ni-LaNiO₃-M catalyst has good performance in resisting carbon deposits.

The XRD results in Figure 1 exhibited broad and weak diffraction peaks for Ni in used 50% Ni-LaNiO₃-M catalysts, indicating that the small particle size of nickel allowed them to stay in this catalyst. Furthermore, the peaks of Ni in used 50% Ni-LaNiO₃-M are similar to that of reduced 50% Ni-LaNiO₃-M, indicating that the active component did not grow during the stability test. As given in Table 2, Ni crystal sizes as calculated from XRD patterns using Scherrer's equation were 4.5 and 4.3 nm for the used and reduced 50% Ni-LaNiO₃-M, respectively. In other words, the 50% Ni-LaNiO₃-M catalyst had good resistance to sintering during the stability test. Similar phenomena can be verified in TEM results.

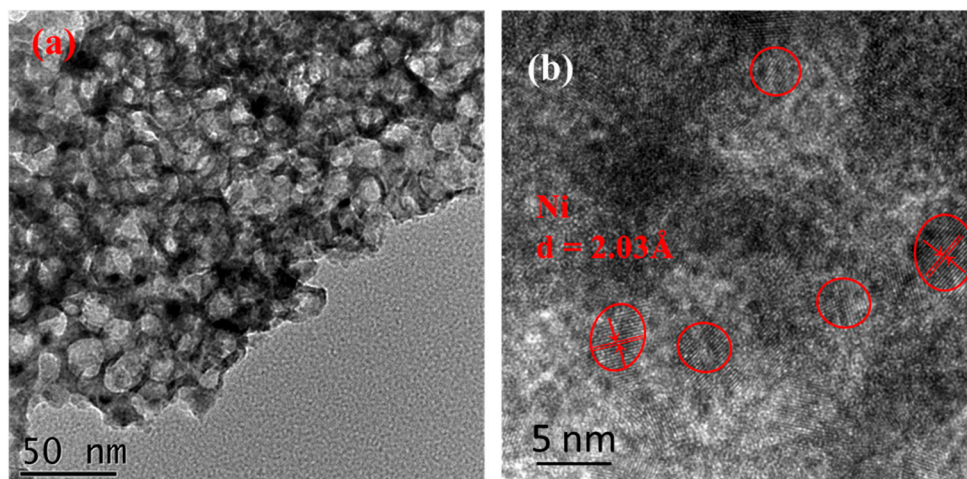


Figure 7. TEM images of the catalysts after stability test: (a,b) 50% Ni-La₂O₃-M and (c,d) 50% Ni-La₂O₃.

TEM and HR-TEM images of the used 50% Ni-La₂O₃-M are shown in Figure 7. The ordered mesoporous structure was well maintained and the lattice distance of 2.03 Å corresponds to the lattice parameters for Ni (111) [32]. Meanwhile, it can be observed that the Ni particle size of 50% Ni-La₂O₃-M was centered around 4.5 nm and that no sintering occurred during the stability test.

Summarizing Section 3.2, the catalyst of 50% Ni-La₂O₃-M performs well in terms of CO₂ methanation activity, and the stability test demonstrated that it has superior activity and excellent selectivity. The XRD and TEM results demonstrate that 50% Ni-La₂O₃-M possessed an ordered mesoporous structure, and that the Ni particle size was small. Meanwhile, the TEM results demonstrate that the catalyst prepared by colloidal solution combustion shows good resistance to carbon deposition. Combining the characterization of 50% Ni-La₂O₃-M with its good performance results, we concluded that the improved activity and stability of 50% Ni-La₂O₃-M catalysts can be attributed to the small Ni particle size embedded by amorphous La₂O₃, which creates a large amount of interface between the Ni and the La₂O₃ support.

3. Materials and Methods

3.1. Synthesis of Catalysts

We used the colloidal solution combustion method to prepare 50% Ni-La₂O₃-M catalysts. During the combustion reaction, glycine (NH₂NH₂COOH) was used as fuel, and metal nitrates (nickel nitrate and lanthanum nitrate) were used as oxidant. Aqueous colloidal SiO₂ LUDOX TMA (Sigma-Aldrich, Saint Louis, USA, 34 wt %, diameter of 22 nm) was used as a hard template to create pores. Typically, La(NO₃)₃·6H₂O (1.33 g), Ni(NO₃)₂·6H₂O (2.48 g), and glycine (0.60 g) were added to deionized water (6.30 mL). After stirring the solution for 10 min and ultrasonic dispersion for 20 min, colloidal SiO₂ (1.26 mL) was added and subjected to ultrasound for 30 min. After this, the solution was transferred onto a hot plate and heated to 200 °C for pyrolysis, during which glycine and nitrate metal undergo a combustion reaction accompanied by the generation of metal oxides and gases. After glycine is fully burned and cooled to room temperature, the metal oxides were calcined at 600 °C for 4 h. The obtained powder was dispersed into a hot NaOH solution to etch the silica. Following this, the powder was washed three times with deionized water and three times with ethanol. After drying at 80 °C for 12 h, 50% Ni-La₂O₃-M catalyst was obtained, with the weight content of Ni being 50%.

For comparison, 50% Ni-La₂O₃ catalysts were prepared by the solution combustion method without adding colloidal SiO₂. The prepared sample was referred to as 50% Ni-La₂O₃.

3.2. Characterization of Catalysts

N₂ isotherms were carried out on an Autosorb-iQ analyzer (Quantachrome Instruments, Boynton Beach, FL, USA) at −196 °C. The catalysts were evaluated at 300 °C for 4 h before the measurements. The BET method was used to calculate the specific surface area. The pore size distributions were obtained from the absorption branch using quenched solid density functional theory (QSDFT). The total pore volumes were calculated according to the adsorption point at P/P₀ = 0.994.

X-ray diffraction (XRD) patterns were obtained on a DX-2700 X-ray diffractometer (Haoyuan Instrument, Dandong, China) with Cu K_α radiation (λ = 0.15406 nm). H₂-temperature programmed reduction (H₂-TPR) was performed on a TP-5080 multifunctional adsorption apparatus (Xianquan, Tianjin, China). A detailed description of the H₂-TPR experiment can be found in our previous publication [33]. H₂-temperature programmed desorption (H₂-TPD) was performed on the same apparatus as H₂-TPR. The catalyst (100 mg), after reduction at 400 °C for 40 min in 5% H₂/Ar, was cooled to room temperature in 5% H₂/Ar. After being purged with pure Ar for 1 h, the catalyst was heated for H₂ desorption from room temperature to 900 °C at a rate of 10 °C/min in pure Ar. Ni dispersion was calculated from the desorption of H₂ using the assumption that the stoichiometric ratio of H/Ni surface is 1. Transmission electron microscope (TEM) images of the catalysts were taken by a Tecnai G2 F20 microscope (FEI Company, Hillsboro, OR, USA).

3.3. Catalytic Performance Test for CO₂ Methanation

Catalytic tests were performed in a fixed-bed reactor (i.d. = 8 mm) at atmospheric pressure in the temperature range of 250–450 °C under a reactant gas flow of 100 mL/min (CO₂/H₂/Ar = 1:4:5). The catalyst sample (50 mg) was diluted with SiO₂ (100 mg) and loaded into the reactor. Before the reaction, the catalyst was reduced at 400 °C in 20% H₂/Ar (50 mL min^{−1}) for 40 min. After reduction, the catalyst was cooled to 250 °C in 20% H₂/Ar. Following this, the reactant gas flow was introduced into the reactor. At each reaction temperature point, the sampling and analysis of reacted gas were conducted after one hour. The stability tests were carried out at 300 °C. The product gas was analyzed using an online gas chromatograph (Techcomp GC-7900, Shanghai, China). CO₂ conversion (X_{CO₂}) and selectivity of CH₄ (S_{CH₄}) were calculated as follows:

$$X_{\text{CO}_2} = \frac{[\text{CO}_2]_{\text{in}} - [\text{CO}_2]_{\text{out}}}{[\text{CO}_2]_{\text{in}}} \times 100\%,$$

$$S_{\text{CH}_4} = \frac{[\text{CH}_4]_{\text{out}}}{[\text{CO}]_{\text{out}} + [\text{CH}_4]_{\text{out}}} \times 100\%,$$

where [CO₂]_{in} and [CO₂]_{out} are the inlet and outlet concentrations of CO₂, respectively. [CH₄]_{out} is the outlet concentration of CH₄.

The turnover frequency (TOF) value, representing the number of converted CO₂ molecules per Ni atom per second, was calculated from the CO₂ conversion and Ni dispersion [34].

Author Contributions: Conceptualization: D.G. and L.W.; Data curation: G.T., D.G. and L.W.; Formal analysis: G.T., H.L. and L.W.; Funding acquisition: H.L. and L.W.; Investigation: G.T., H.L. and L.W.; Writing—original draft: G.G.; Writing—review & editing: H.L. and L.W.

Funding: This research was funded by the Natural Science Foundation of China (No. 21406206), the university students' innovation program of Zhejiang province (No. 2017R411017) and the national university students' innovation and entrepreneurship training program (No. 201710340016).

Acknowledgments: The authors would like to thank Jiliang Yang and Yundi Zhang for help with the experiments and measurements.

Conflicts of Interest: The authors declare no conflict of interest.

References

1. Ma, J.; Sun, N.; Zhang, X.; Zhao, N.; Xiao, F.; Wei, W.; Sun, Y. A short review of catalysis for CO₂ conversion. *Catal. Today* **2009**, *148*, 221–231. [[CrossRef](#)]
2. Wang, Y.; Tan, L.; Tan, M.; Zhang, P.; Fang, Y.; Yoneyama, Y.; Yang, G.; Tsubaki, N. Rationally Designing Bifunctional Catalysts as an Efficient Strategy To Boost CO₂ Hydrogenation Producing Value-Added Aromatics. *ACS Catal.* **2019**, *9*, 895–901. [[CrossRef](#)]
3. Su, X.; Xu, J.; Liang, B.; Duan, H.; Hou, B.; Huang, Y. Catalytic carbon dioxide hydrogenation to methane: A review of recent studies. *J. Energy Chem.* **2016**, *25*, 553–565. [[CrossRef](#)]
4. Rönisch, S.; Schneider, J.; Matthischke, S.; Schlüter, M.; Götz, M.; Lefebvre, J.; Prabhakaran, P.; Bajohr, S. Review on methanation—From fundamentals to current projects. *Fuel* **2016**, *166*, 276–296. [[CrossRef](#)]
5. Karelavic, A.; Ruiz, P. Mechanistic study of low temperature CO₂ methanation over Rh/TiO₂ catalysts. *J. Catal.* **2013**, *301*, 141–153. [[CrossRef](#)]
6. Swalus, C.; Jacquemin, M.; Poleunis, C.; Bertrand, P.; Ruiz, P. CO₂ methanation on Rh/γ-Al₂O₃ catalyst at low temperature: “In situ” supply of hydrogen by Ni/activated carbon catalyst. *Appl. Catal. B* **2012**, *125*, 41–50. [[CrossRef](#)]
7. Sharma, S.; Hu, Z.; Zhang, P.; McFarland, E.W.; Metiu, H. CO₂ methanation on Ru-doped ceria. *J. Catal.* **2011**, *278*, 297–309. [[CrossRef](#)]
8. Kim, H.Y.; Lee, H.M.; Park, J.-N. Bifunctional Mechanism of CO₂ Methanation on Pd-MgO/SiO₂ Catalyst: Independent Roles of MgO and Pd on CO₂ Methanation. *J. Phys. Chem. C* **2010**, *114*, 7128–7131. [[CrossRef](#)]
9. Razaq, R.; Li, C.; Usman, M.; Suzuki, K.; Zhang, S. A highly active and stable Co₄N/γ-Al₂O₃ catalyst for CO and CO₂ methanation to produce synthetic natural gas (SNG). *Chem. Eng. J.* **2015**, *262*, 1090–1098. [[CrossRef](#)]
10. Schubert, M.; Pokhrel, S.; Thomé, A.; Zielasek, V.; Gesing, T.M.; Roessner, F.; Mädler, L.; Bäumer, M. Highly active Co–Al₂O₃-based catalysts for CO₂ methanation with very low platinum promotion prepared by double flame spray pyrolysis. *Catal. Sci. Technol.* **2016**, *6*, 7449–7460. [[CrossRef](#)]
11. Liu, H.; Xu, S.; Zhou, G.; Huang, G.; Huang, S.; Xiong, K. CO₂ hydrogenation to methane over Co/KIT-6 catalyst: Effect of reduction temperature. *Chem. Eng. J.* **2018**, *351*, 65–73. [[CrossRef](#)]
12. Bian, Z.; Chan, Y.M.; Yu, Y.; Kawi, S. Morphology dependence of catalytic properties of Ni/CeO₂ for CO₂ methanation: A kinetic and mechanism study. *Catal. Today* **2018**. [[CrossRef](#)]
13. Le, T.A.; Kim, T.W.; Lee, S.H.; Park, E.D. Effects of Na content in Na/Ni/SiO₂ and Na/Ni/CeO₂ catalysts for CO and CO₂ methanation. *Catal. Today* **2018**, *303*, 159–167. [[CrossRef](#)]
14. Le, T.A.; Kim, M.S.; Lee, S.H.; Kim, T.W.; Park, E.D. CO and CO₂ methanation over supported Ni catalysts. *Catal. Today* **2017**, *293–294*, 89–96. [[CrossRef](#)]
15. Stangeland, K.; Kalai, D.; Li, H.; Yu, Z. CO₂ Methanation: The Effect of Catalysts and Reaction Conditions. *Energy Procedia* **2017**, *105*, 2022–2027. [[CrossRef](#)]
16. Liu, Q.; Tian, Y. One-pot synthesis of NiO/SBA-15 monolith catalyst with a three-dimensional framework for CO₂ methanation. *Int. J. Hydrog. Energy* **2017**, *42*, 12295–12300. [[CrossRef](#)]
17. Chen, C.-S.; Budi, C.S.; Wu, H.-C.; Saikia, D.; Kao, H.-M. Size-Tunable Ni Nanoparticles Supported on Surface-Modified, Cage-Type Mesoporous Silica as Highly Active Catalysts for CO₂ Hydrogenation. *ACS Catal.* **2017**, *7*, 8367–8381. [[CrossRef](#)]
18. Bacariza, M.C.; Graça, I.; Bebiano, S.S.; Lopes, J.M.; Henriques, C. Micro- and mesoporous supports for CO₂ methanation catalysts: A comparison between SBA-15, MCM-41 and USY zeolite. *Chem. Eng. Sci.* **2018**, *175*, 72–83. [[CrossRef](#)]
19. Sun, X.; Suarez, A.I.O.; Meijerink, M.; van Deelen, T.; Ould-Chikh, S.; Zečević, J.; de Jong, K.P.; Kapteijn, F.; Gascon, J. Manufacture of highly loaded silica-supported cobalt Fischer–Tropsch catalysts from a metal organic framework. *Nat. Commun.* **2017**, *8*, 1680. [[CrossRef](#)]
20. Garbarino, G.; Wang, C.; Cavattoni, T.; Finocchio, E.; Riani, P.; Flytzani-Stephanopoulos, M.; Busca, G. A study of Ni/La-Al₂O₃ catalysts: A competitive system for CO₂ methanation. *Appl. Catal. B* **2019**, *248*, 286–297. [[CrossRef](#)]
21. Song, H.; Yang, J.; Zhao, J.; Chou, L. Methanation of Carbon Dioxide over a Highly Dispersed Ni/La₂O₃ Catalyst. *Chin. J. Catal.* **2010**, *31*, 21–23. [[CrossRef](#)]
22. Li, X.; Li, D.; Tian, H.; Zeng, L.; Zhao, Z.-J.; Gong, J. Dry reforming of methane over Ni/La₂O₃ nanorod catalysts with stabilized Ni nanoparticles. *Appl. Catal. B* **2017**, *202*, 683–694. [[CrossRef](#)]

23. Voskanyan, A.A.; Chan, K.-Y.; Li, C.-Y.V. Colloidal Solution Combustion Synthesis: Toward Mass Production of a Crystalline Uniform Mesoporous CeO₂ Catalyst with Tunable Porosity. *Chem. Mater.* **2016**, *28*, 2768–2775. [[CrossRef](#)]
24. Wang, L.; Liu, H. Mesoporous Co-CeO₂ catalyst prepared by colloidal solution combustion method for reverse water-gas shift reaction. *Catal. Today* **2018**, *316*, 155–161. [[CrossRef](#)]
25. Leofanti, G.; Padovan, M.; Tozzola, G.; Venturelli, B. Surface area and pore texture of catalysts. *Catal. Today* **1998**, *41*, 207–219. [[CrossRef](#)]
26. Neimark, A.V.; Lin, Y.; Ravikovitch, P.I.; Thommes, M. Quenched solid density functional theory and pore size analysis of micro-mesoporous carbons. *Carbon* **2009**, *47*, 1617–1628. [[CrossRef](#)]
27. Tada, S.; Shimizu, T.; Kameyama, H.; Haneda, T.; Kikuchi, R. Ni/CeO₂ catalysts with high CO₂ methanation activity and high CH₄ selectivity at low temperatures. *Int. J. Hydrog. Energy* **2012**, *37*, 5527–5531. [[CrossRef](#)]
28. Pereñíguez, R.; González-DelaCruz, V.M.; Holgado, J.P.; Caballero, A. Synthesis and characterization of a LaNiO₃ perovskite as precursor for methane reforming reactions catalysts. *Appl. Catal. B* **2010**, *93*, 346–353. [[CrossRef](#)]
29. Zou, Y.; Wang, Y. NiO nanosheets grown on graphene nanosheets as superior anode materials for Li-ion batteries. *Nanoscale* **2011**, *3*, 2615–2620. [[CrossRef](#)] [[PubMed](#)]
30. Li, S.; Tang, H.; Gong, D.; Ma, Z.; Liu, Y. Loading Ni/La₂O₃ on SiO₂ for CO methanation from syngas. *Catal. Today* **2017**, *297*, 298–307. [[CrossRef](#)]
31. Xue, Y.; Yan, C.; Zhao, X.; Huang, S.; Guo, C. Ni/La₂O₃-ZrO₂ catalyst for hydrogen production from steam reforming of acetic acid as a model compound of bio-oil. *Korean J. Chem. Eng.* **2017**, *34*, 305–313. [[CrossRef](#)]
32. Nuvula, S.; Sagar, T.V.; Valluri, D.K.; Sai Prasad, P.S. Selective substitution of Ni by Ti in LaNiO₃ perovskites: A parameter governing the oxy-carbon dioxide reforming of methane. *Int. J. Hydrog. Energy* **2018**, *43*, 4136–4142. [[CrossRef](#)]
33. Wang, L.; Liu, H.; Ye, H.; Hu, R.; Yang, S.; Tang, G.; Li, K.; Yang, Y. Vacuum Thermal Treated Ni-CeO₂/SBA-15 Catalyst for CO₂ Methanation. *Nanomaterials* **2018**, *8*, 759. [[CrossRef](#)] [[PubMed](#)]
34. Li, S.; Guo, S.; Gong, D.; Kang, N.; Fang, K.-G.; Liu, Y. Nano composite composed of MoO_x-La₂O₃-Ni on SiO₂ for storing hydrogen into CH₄ via CO₂ methanation. *Int. J. Hydrog. Energy* **2019**, *44*, 1597–1609. [[CrossRef](#)]



© 2019 by the authors. Licensee MDPI, Basel, Switzerland. This article is an open access article distributed under the terms and conditions of the Creative Commons Attribution (CC BY) license (<http://creativecommons.org/licenses/by/4.0/>).